

Laboratory study on the modulation evolution of nonlinear wave trains

G.H. Dong^{*1}, Y.X. Ma¹, W. Zhang¹ and X.Z. Ma^{1,2}

¹*State Key Laboratory Of Coastal And Offshore Engineering, Dalian University Of Technology, Dalian 116023, China*

²*State Key Laboratory of Hydrology-Water Resources and Hydraulic Engineering, Hohai University, Nanjing 210098, P. R. China*

(Received March 26, 2012, Revised July 9, 2012, Accepted July 31, 2012)

Abstract. New experiments focusing on the evolution characteristics of nonlinear wave trains were conducted in a large wave flume. A series of wave trains with added sidebands, varying initial steepness, perturbed amplitudes and frequencies, were physically generated in a long wave flume. The experimental results show that the increasing wave steepness, increases the speed of sidebands growth. To study the frequency and phase modulation, the Morlet wavelet transform is adopted to extract the instantaneous frequency of wave trains and the phase functions of each wave component. From the instantaneous frequency, there are local frequency downshifts, even an effective frequency downshift was not observed. The frequency modulation increases with an increase in amplitude modulation, and abrupt changes of instantaneous frequencies occur at the peak modulation. The wrapped phase functions show that in the early stage of the modulation, the phase of the upper sideband first diverges from that of the carrier waves. However, at the later stage, the discrepancy phase from the carrier wave transformed to the lower sideband. The phase deviations appear in the front of the envelope's peaks. Furthermore, the evolution of the instantaneous frequency exhibits an approximate recurrence-type for the experiment with large imposed sidebands, even when the corresponding recurrence is not observed in the Fourier spectrum.

Keywords: nonlinear waves; evolution; modulation instability; instantaneous frequency; spectra; wavelet transform

1. Introduction

Benjamin and Feir (1967) theoretically demonstrated that a deep-water Stokes wave is unstable to small disturbances due to higher-order de-tuning resonant wave interactions, the amplitudes of the disturbances growing exponentially along with the wave propagation, and the growth rate of the sidebands being proportional to the square of the wave steepness. This unstable phenomenon was experimentally confirmed by Benjamin (1967) and was then called Benjamin-Feir (B-F) instability or the modulational instability. After the milestone work of Benjamin and Feir (1967), many studies were carried out to further investigate the characteristics of the modulational instability mainly by experimental (Lake *et al.* 1977, Melville 1982, Tulin and Waseda 1999, Hwung *et al.* 2007) and theoretical (Chu and Mei 1970, Dysthe 1979, Kharif *et al.* 2010, Longuet-Higgins 1980, Trulsen

*Corresponding author, Professor, E-mail: ghdong@dlut.edu.cn

and Dysthe 1996, Zakharov 1968) approaches.

Zakharov (1968) illustrated that the evolution of deep-water narrow band waves can be described well by the nonlinear Schrödinger equation (NLS). Currently, most researches regarding the modulational instability of deep water gravity waves are carried out in the framework of the NLS equations. Although great progress has been obtained with this approach (Lake *et al.* 1978, Lo and Mei 1985, Segur *et al.* 2005), experimental studies are lacking.

Lake *et al.* (1977) was first experimentally verified the B-F instability theory and observed that the lower sideband amplitude can exceed that of the initial carrier wave (i.e., the frequency downshift phenomenon) and the evolution of non-breaking wave trains exhibited an approximate recurrence-type. The perfect recurrence can also be demonstrated by the NLS equations (Lo and Mei 1985). Melville (1982) conducted experiments with initially uniform wave trains and found that the frequency downshift occurred after wave breaking. Later, Melville (1983) analyzed the process of deep-water wave modulation in detail using the Hilbert transform, and used *phase reversals* (the local large instantaneous phase change) to explain the frequency downshift that appeared after wave breaking. This study found that *phase reversal* corresponded to waves with amplitudes close to zero.

Tulin and Waseda (1999) systematically analyzed the modulational instability evolution in a large wave flume using wave trains with initially imposed sidebands. The breaking events during the wave modulation were discussed in detail in these experiments. Recently, Hwung *et al.* (2007) conducted a series of experiments in a long wave flume with a length of 300 m; thus, the modulation characteristics in the later stage could be observed. Hwung *et al.* (2007) found that waves with initial steepness less than 0.11 exhibited a recurrence-type evolution; however, for wave trains with larger steepness, the modulational instability eventually resulted in breaking. Additionally, these experiments showed that the frequency downshift that occurred after breaking was not permanent.

Although great progress has been made in the previous experimental studies, there are still certain aspects that have not been clearly understood, such as the instantaneous frequency evolution and the phase function variations during the evolution process. These aspects are the primary motivation of this research. The evolution of the instantaneous frequencies and phases is crucial for understanding the characteristics of the modulational instability. The traditional method to extract the instantaneous frequency and phase by the Hilbert transform (Melville 1983) cannot obtain the instantaneous frequency and the phases exactly (Ma *et al.* 2010). In this study, the Morlet wavelet transform is used to study the instantaneous frequency and phases. From Hwung *et al.* (2007) and Ma *et al.* (2010) the method based on the Morlet transform can obtain the instantaneous frequency reasonably.

In this study, a series of wave trains with added sidebands, varying initial steepness, and perturbed amplitudes and frequencies are physically generated in a long wave flume. Following this introduction, the experimental set-up and analysis methods are introduced in Section 2. A detailed discussion of the results is given in Section 3. Lastly, in Section 4, the conclusions of this research are presented.

2. Experimental set-up and data analysis

2.1 Experimental set-up

2.1.1 Wave flume

The experiments were conducted in the wave flume at the State Key Laboratory of Coastal and

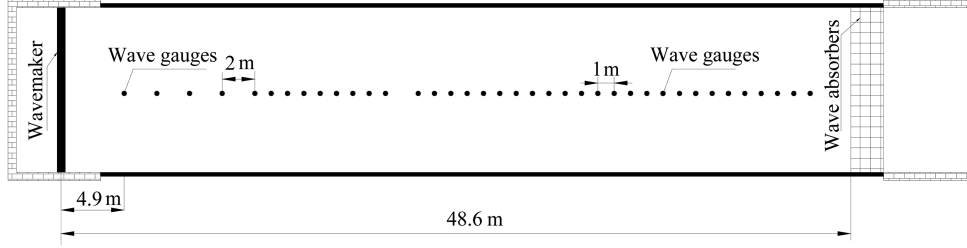


Fig. 1 Sketch diagram of the experimental set-up

Offshore Engineering, Dalian University of Technology, Dalian, China. This flume is 65 m long, 2 m wide, 1.8 m high and was used with a water depth of 1 m. The detailed experimental set-up is shown in Fig. 1. The flume is equipped with a hydraulically driven piston-type wavemaker and in the following $x = 0$ m is defined as the mean position of the wave maker. At another end of the tank wave absorbers were installed to mitigate the wave reflection. Prior tests indicated that the reflection of the flume for the waves used herein is less than 5%, thus the reflection effect can be neglected. The water surface elevations were recorded simultaneously with 35 capacitance wave gauges, which are delineated by filled circles in Fig. 1. The absolute accuracy of these wave gauges was of the order of ± 1 mm. Before any experiments, these wave gauges were examined for soundness, cleaned if necessary, and then calibrated.

In a physical wave flume, viscous dissipation due to sidewalls is ubiquitous (Banner and Peirson 2007, Tian *et al.* 2010). Experiments without breaking show that the energy dissipation along the flume is approximately 18%.

2.1.2 Wave generation

In this work, the evolution of wave trains with imposed sidebands are examined. In this way, the background noise of the flume can be greatly suppressed (Tulin and Waseda 1999). A wave train with imposed sidebands can be expressed as follows

$$\eta(t) = a_c \sin(2\pi f_c t) + a_- \sin(2\pi f_- t + \phi_-) + a_+ \sin(2\pi f_+ t + \phi_+) \quad (1)$$

$$f_{\pm} = f_c + \delta f \quad (2)$$

$$a = \sqrt{a_c^2 + a_+^2 + a_-^2} \quad (3)$$

where η denotes the wave surface elevation, a_c , a_+ and a_- are the amplitudes of the carrier, upper sideband and lower sideband, respectively, f_c , f_+ and f_- are the corresponding cyclic frequencies, δf is the frequency difference between the carrier wave and its sidebands, and ϕ_+ and ϕ_- are the initial phases of the sidebands. To provide the maximum growth rate, ϕ_{\pm} are set to $-\pi/4$ (Benjamin and Feir 1967). And a is the equivalent wave amplitude. A number of experimental cases of nonlinear wave trains with different initial wave steepness $\varepsilon = ka$ (k is the wave number) and perturbation amplitudes were generated. The detailed wave group parameters for certain cases are described in Table. 1.

To reduce the effect of wave fronts, a finite ramp $e(t)$ is added at the beginning and end of the wave generation signals, as described by Tulin and Waseda (1999)

Table 1 Wave group parameters

Case	f_c	δf (Hz)	kh	ε	a_{\pm}/a_0	
SB1	1.00	0.10	4.03	0.13	0.05	No
SB2	1.00	0.10	4.03	0.19	0.05	Yes
SB3	1.00	0.10	4.03	0.23	0.05	Yes
SB4	1.25	0.10	6.30	0.13	0.50	Yes

$$\psi(t) = \begin{cases} \frac{1}{2}(1 - \cos(\pi t/\tau)), & 0 \leq t \leq \tau \\ 1 & \tau < t < T - \tau \\ \frac{1}{2}(1 - \cos(\pi t/\tau)), & T - \tau < t \leq T \end{cases} \quad (4)$$

where τ is the ramp duration and T is the total duration of the signal.

2.2 Data analysis method

2.2.1 Wave spectra

Wave spectra can describe the energy distribution as a function of frequency. From the spectrum, the evolution of the frequency components energy can be detected. In this study, wave spectra $A(f)$ were obtained by fast Fourier Transform (FFT) and then smoothed with the Hanning window. The frequency resolution of the spectra is approximately 0.012 Hz, which is small enough to distinguish adjacent wave modes.

From the wave spectra, the amplitudes of each frequency mode a_n can be estimated as the square root of the energy of the spectral peaks by integrating the contributions from the neighboring frequency bins

$$a_n^2 = \left[\frac{1}{2}(A_{n-1}^2 + A_{n+1}^2) + A_n^2 \right] \quad (5)$$

by doing this, the leakage of spectral energy due to finite length of the recorded time series can be compensated to some extent.

2.2.2 Instantaneous frequency extraction

Investigating the variations of instantaneous frequencies of time series is a convenient way to study the characteristic of the frequency modulation. The method for extracting instantaneous frequency from the wavelet transform is adopted herein.

The wavelet transform of a time series $x(t)$ is defined as

$$WT(a, \tau) = \int_{-\infty}^{\infty} x(t) \psi_{a, \tau}^*(t) dt \quad (6)$$

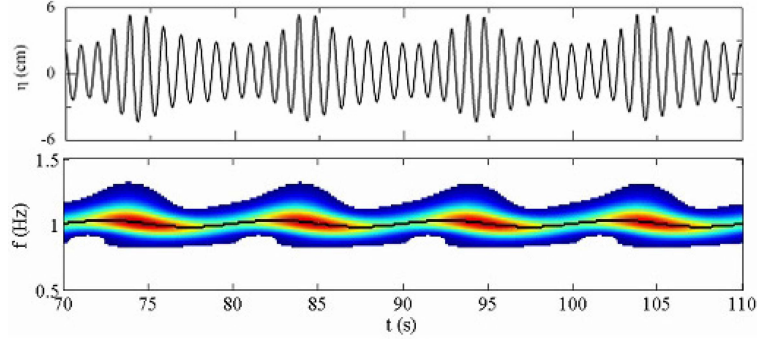


Fig. 2 The surface elevations (upper) and the corresponding wavelet spectrum (lower) for a wave train ($\varepsilon = 0.13$, $f_c = 1.0$ Hz and $\delta f = 0.1$) with imposed sidebands. The black solid line in the lower panel represents the instantaneous frequencies

where the asterisk denotes the complex conjugate and $\psi_{a,\tau}(t)$ represents a family of functions called wavelets that are constructed by translating in time, τ and dilation with scale, a , a mother wavelet function $\psi(t)$. The scale a can be interpreted as the reciprocal of frequency, $f = 1/a$. One of the most extensively used mother wavelets in harmonic analysis is the Morlet wavelet (Masset 2001); it is a plane analytical wave modulated by a Gaussian envelope and is defined as

$$\psi(t) = \pi^{-1/4} \exp\left(-\frac{t^2}{2}\right) \exp(i\omega_0 t) \quad (7)$$

where ω_0 is the peak frequency of the wavelet, usually chosen to be 6.0 (Farge 1992). Due to the multi-analytical characteristic of the Morlet wavelet transform, the wavelet coefficients at each scale are actually the corresponding analytical signal, thus, the phase functions of each wave component can also be obtained. Hence, the process for filter the signal before Hilbert transform used by Banner and Tian (1998) and Tian *et al.* (2008) can be ignored.

The wavelet energy spectrum $P(s,t)$ can be defined as

$$P(s,t) = \frac{|WT(s,t)|^2}{s} \quad (8)$$

At any time t_n , the scale with the largest energy can be regard as the reciprocal of the instantaneous frequency (Ma *et al.* 2010). An illustration for this method to extract the instantaneous frequencies can be seen in Fig. 2.

3. Results discussion

3.1 The effects of initial wave steepness

Previous studies indicated that the initial steepness of wave trains play an important role in the modulation evolution. Figs. 3-5 illustrate the evolution of wave trains with the same carrier wave, perturbed frequency and initial modulation rate ($f_c = 1.0$ Hz, $\delta f = 0.1$ and $a_{\pm}/a_0 = 0.05$, respectively), but different initial wave steepness. For a convenient comparison, wave spectra in both the semi-

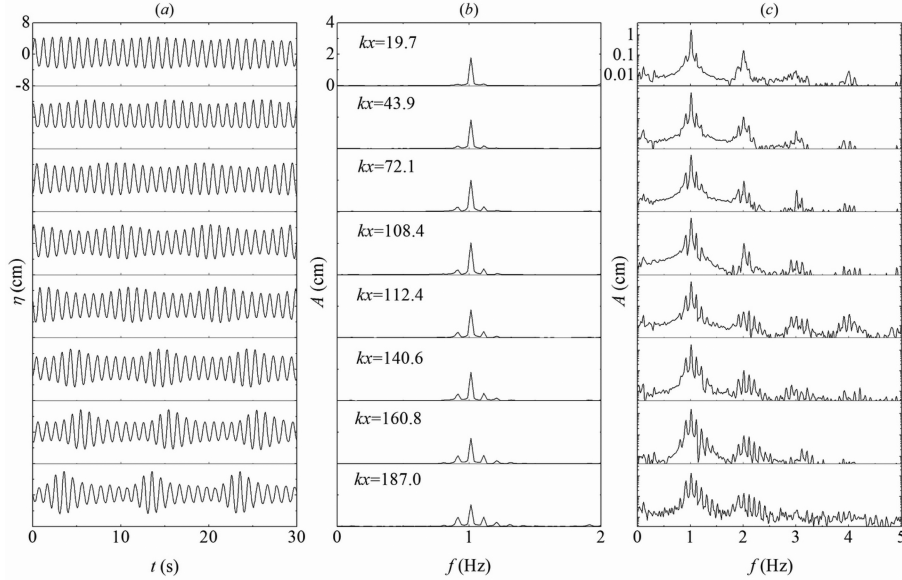


Fig. 3 The evolution of the wave train with $f_c = 1.0$ Hz, $\varepsilon = 0.13$, $\delta f = 0.1$ Hz and $a_{\pm}/a_0 = 0.05$: (a) surface elevations, (b) wave amplitude spectra in the liner coordinates and (c) wave amplitude spectra in the semi-log coordinates

logarithmic and the linear coordinates are presented.

The right panels in Fig. 3 represent the measured surface elevations at select locations of waves with an initial steepness of $\varepsilon = 0.13$. Breaking was not observed during this evolution. It should be noted that breaking was observed in the evolution of waves with a similar initial steepness in the previous experiments (Tulin and Waseda 1999, Chiang and Hwung 2007). The difference in results is mainly caused by the non-negligible dissipation of the present flume. According to the theory of Segur *et al.* (2005), the modulation evolution of the waves train may be bounded by the dissipation. Thus, breaking events were not observed during the evolution of the wave train.

With the increase of propagation distance, the amplitude modulation of the wave train is clearer. At the last location ($kx = 187.0$), the degree of the modulation still increased; however, because of the length limitation of the flume, the subsequent evolution of the wave train was not observed. The corresponding spectra also reflect the evolution of waves. The sidebands had minimal growth until $kx > 43.9$. With the increase of the propagation distance, the sidebands obtain energy from the expended energy of the carrier wave. Along the flume, the growth rate of both sidebands is the same, i.e., there is no obvious asymmetry growth of the imposed sidebands. Meanwhile, the bound higher harmonics ($2f_c$, $3f_c$) and its corresponding sidebands also increased. In the experiment of Chiang and Hwung (2007), at the location $kx = 187$, the wave trains with an initial steepness of about 0.13 also did not show asymmetrical growth between the lower and higher sidebands.

It should be noted that, due to the resonance wave interactions, at $kx > 112.4$, there was growth of the free waves with $f_{c \pm n\delta f}$ ($n \geq 2$). At the end of the flume, the growth of the free high-frequency waves is more obvious than that of the low-frequency waves, especially for waves beyond $f_c - 2\delta f$. The physical mechanics of the growth of the waves of $f_{c \pm n\delta f}$ can be explained as these frequencies combining with the initial waves to satisfy the condition of Benjamin-Feir instability. However, the reason for the asymmetrical growth at the free waves of $f_{c \pm n\delta f}$ ($n \geq 3$) is not clear. Tulip and

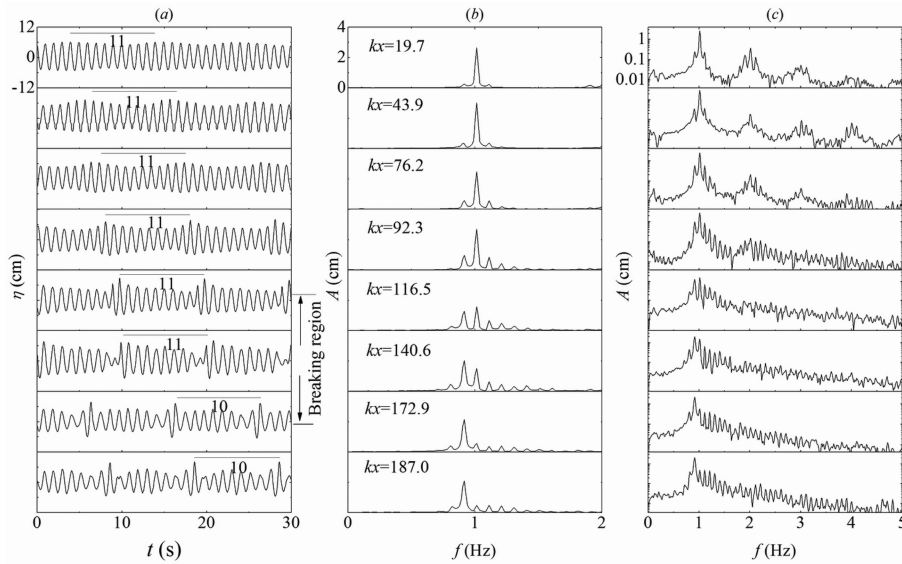


Fig. 4 The evolution of the wave trains with $f_c = 1.0$ Hz, $\varepsilon = 0.19$, $\delta f = 0.1$ Hz and $a_{\pm}/a_0 = 0.05$: (a) surface elevations, (b) wave amplitude spectrum in the liner coordinates and (c) wave amplitude spectrum in the semi-log coordinates

Waseda (1999) gave an explanation that this phenomenon can be mainly attributed to the asymmetrical growth of the primary sidebands. However, in this case, the primary upper and lower sidebands do not show obvious asymmetrical growth, indicating the explanation of Tulip and Waseda (1999) cannot be applied here.

The evolution of the wave trains with a larger initial steepness ($\varepsilon = 0.19$) is shown in Fig. 4. The modulation of this experimental case is faster than that of the previously discussed case, and the initial breaking was observed at $kx = 116.5$, with a local maximum steepness $\varepsilon = 0.42$ ($\varepsilon = k_p a_m$, where k_p is the local wave number corresponding to the peak amplitude and a_m is peak crest), which is very close to the theoretical extreme Stokes wave and the previous experiments (Tulin and Waseda 1999). After wave breaking, the continuous wave train is disintegrated to a series of wave groups. The amplitudes of the waves between the adjacent wave groups are close to zero. However, as the waves propagate further, the wave train becomes continuous again. For this case, the growth of the sidebands can be clearly observed with the Fourier spectra. The amplitude of the lower sideband is larger than that of the higher sideband from $kx = 140.6$. After wave breaking, the asymmetrical growth is more evident and the amplitude of the lower sideband exceeds the carrier wave, becoming the dominant wave in the frequency domain; thus, an effective frequency downshift occurred. Simultaneously, the numbers of waves per group decreased from 11 to 10, corresponding to an effective frequency downshift (the middle panel of Fig. 4). Additionally, in the case, the growth of the free high-frequency waves also outstrips the low-frequency waves.

The evolution results for the case with the maximum steepness ($\varepsilon = 0.23$) in this discussion are provided in Fig. 5. This case illustrates a faster modulation process, in which the initial breaking occurred at $kx = 72.1$ with a local maximum steepness $\varepsilon = 0.437$. Due to the width of the flume, the breaking events for this case demonstrated three dimensional features. Breaking occurred not only at the crest of the waves, also occurred near the sidewalls. This three-dimensional breaking type may

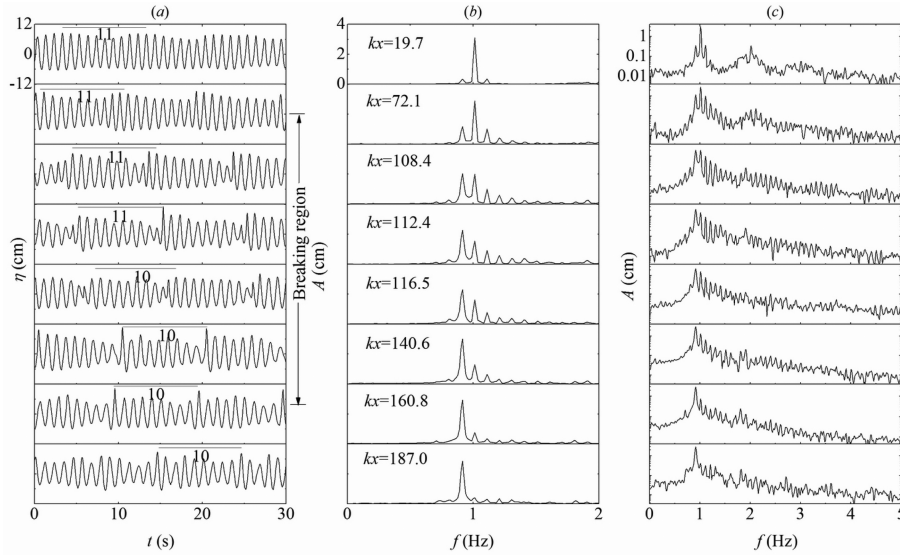


Fig. 5 The evolution of the wave trains with $f_c = 1.0$ Hz, $\varepsilon = 0.23$, $\delta f = 0.1$ Hz and $a_{\pm}/a_0 = 0.05$: (a) surface elevations, (b) wave amplitude spectrum in the liner coordinates and (c) wave amplitude spectrum in the semi-log coordinates

be caused by the three-dimensional instability, which was also observed in the previous experiments (Su 1982, Waseda and Tulin 1999). After wave breaking, an effective frequency downshift is observed. At the end of the flume, the shape of the wave train demonstrates a demodulation (again becoming a near uniform wave train again). However, the evolution in the frequency domain does not show a similar trend.

Comparing with the evolution of the waves in Figs. 3-5, with increasing of initial steepness, the modulation is more obvious and breaking occurs earlier. Additionally, wave breaking can accelerate the growth rate of the lower sideband, while suppressing the growth of the higher sideband. With the increase of the initial steepness, the wave spectra in the semi-log coordinates indicate that the generation of the free waves at discrete frequencies tends to spread to a continuous frequency band, suggesting that the initial steepness is important for the mechanism of continuous or discrete development.

There is currently no detailed discussion regarding the time and frequency domain. However, the variations of frequencies and phases in the time domain are not yet clear. In this section, the frequency modulation and the phase function variations for two experimental cases, which are corresponding to the wave trains with the smallest (Fig. 3) and largest (Fig. 5) initial steepness, will be illustrated.

Fig. 6 shows the evolution of the instantaneous peak frequencies along the flume for the case with the initial steepness $\varepsilon = 0.13$ (corresponding to the experimental case in Fig. 3). For convenient comparison, the measured surface elevations are also presented. At $kx < 19.7$, the instantaneous peak frequency of the wave train mainly concentrates in the carrier frequency f_c . At $kx = 72.1$, small deviations from f_c appear at certain time intervals. At $kx = 108.4$, the instantaneous peak frequencies show obvious modulation with higher frequencies at the crests of the surface envelope and lower frequencies at the troughs of the envelope. The amplitude of the frequency modulation increases

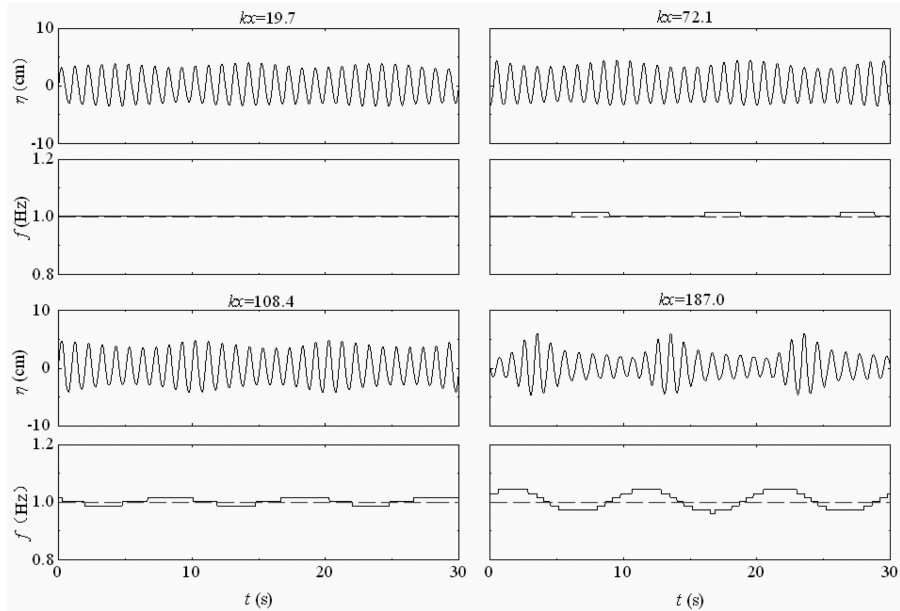


Fig. 6 The evolution of the instantaneous frequencies for the wave train ($f_c = 1.0$ Hz, $\varepsilon = 0.13$, $\delta f = 0.1$ and $a_{\pm}/a_0 = 0.05$); The dash line represents the initial peak wave frequency f_c

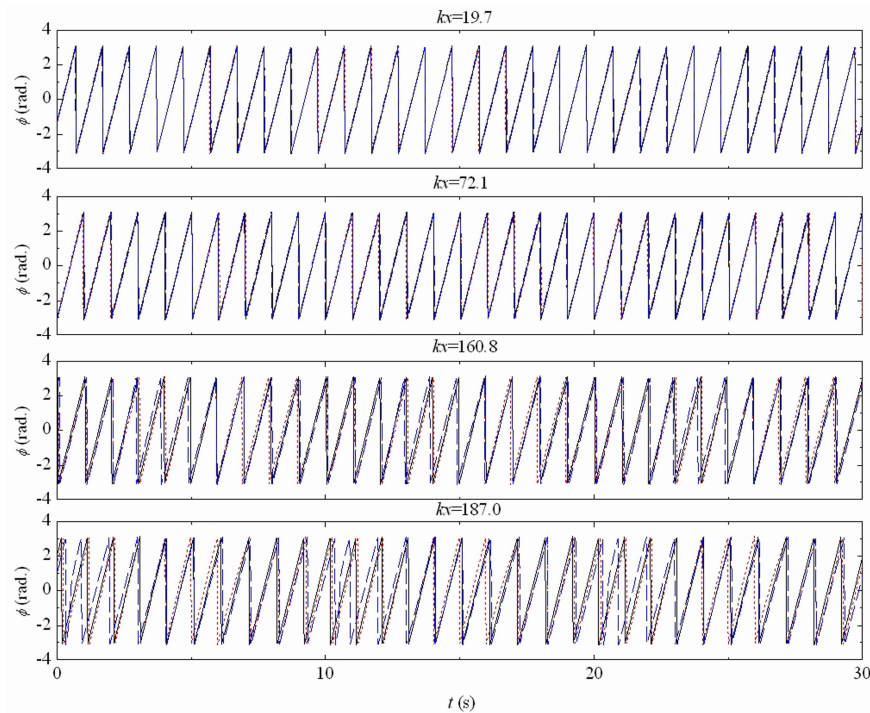


Fig. 7 The wrapped phase functions of the wave trains ($f_c = 1.0$ Hz, $\varepsilon = 0.23$, $\delta f = 0.1$ and $a_{\pm}/a_0 = 0.05$); The dot line is the lower sideband phase function, the solid line is the carrier wave phase function and the blue dash line is the upper sideband phase

with increasing propagation distance. The instantaneous peak frequencies illustrate both local frequency downshift and upshift, although effective frequency downshift was not observed for this case. As waves with a lower frequency propagate faster, the local maximum crests can continuously increase due to the “chasing process” of waves with different frequencies corresponding to a linear aspect. Besides, the increase of the frequency modulation indicates that the increase of the maximum amplitude may also be due to a nonlinear process.

The wrapped phase functions for the three wave components of this experimental case are shown in Fig. 7. The three phase functions coincide with each other at the locations without frequency modulation. Whereas, the upper sideband phase deviates the carrier waves at $kx = 108.4$, where the frequency modulation occurs.

The frequency modulation of the wave train with a larger steepness $\varepsilon = 0.23$ is shown in Fig. 8. Before the initial breaking ($kx < 72.1$), similar to the case with a smaller initial steepness, the amplitude of the frequency modulation increases with the propagation distance, as does the local maximum amplitude. The breaking events occurred intermittently ($72.1 < kx < 160.8$) at the downstream direction. At the initial breaking location ($kx = 72.1$), the oscillation of the

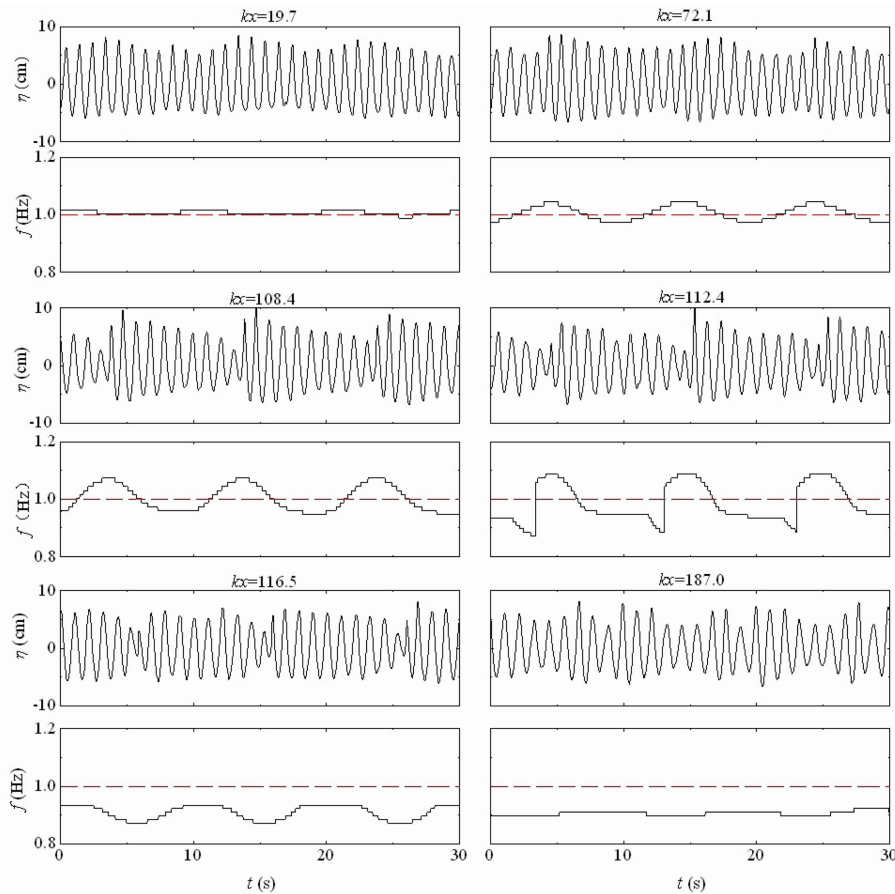


Fig. 8 The evolution of the instantaneous frequency for the wave train ($f_c = 1.0$ Hz $\varepsilon = 0.23$, $\delta f = 0.1$ and $a_{\pm}/a_0 = 0.05$); The dash line represents the initial peak wave frequency f_0

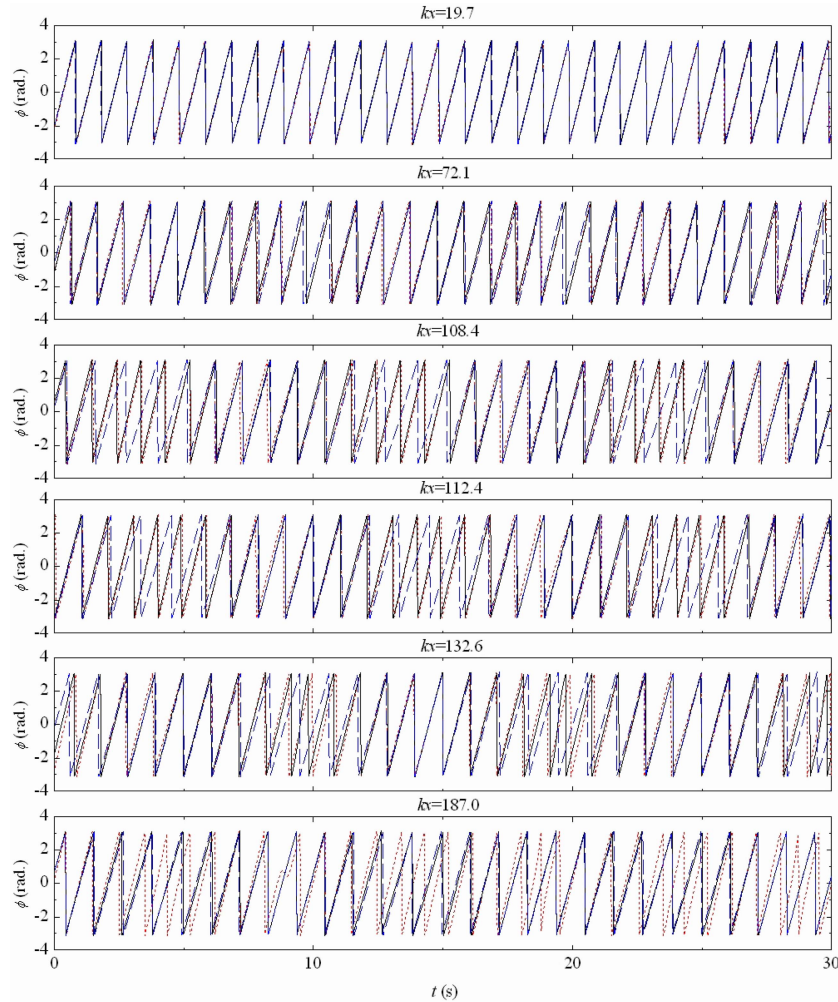


Fig. 9 The wrapped phase functions of the wave trains ($f_c = 1.0$ Hz, $\varepsilon = 0.23$, $\delta f = 0.1$ and $a_\pm/a_0 = 0.05$); The dot line is the lower sideband phase function, the solid line is the carrier wave phase function and the blue dash line is the upper sideband phase

instantaneous frequency follows a Stokes-type shape, i.e., a sharp crest and a gentle trough, and the modulation amplitude increases in the downstream locations. At $kx = 112.4$, however, the peak frequency oscillation is very steep. There are abrupt local ($t = 13$ s, 23 s) frequency downshifts at this location, and the time regions with the abrupt changes correspond to waves with small amplitudes. After wave breaking, the instantaneous frequencies shift to the lower side of the initial peak frequency and oscillate around the initial lower sideband frequency ($f_c - \delta f$). Outside the breaking region, the modulation of the frequency gradually becomes weak. At the end of the flume, the peak frequencies mainly concentrate at the initial input lower side frequency.

The wrapped phase functions of this case for the carrier wave and the lower and upper sidebands at select measured locations are shown in Fig. 9. At the first measured location ($kx = 19.7$), the phases of the three wave components coincide well. However, similar to the cases with smaller initial steepness, as the waves propagate forward, the phase of the upper sideband first deviated

from the phases of the other two components. This deviation is clearer at the downstream locations. In addition, the deviations correspond to the time intervals before the peak of the surface envelop. At $kx = 140.6$, however, the phase deviations from the initial carrier waves are at the lower sideband, and these deviations correspond to the time intervals with the surface envelop that occurs before the peak amplitude. It is very interesting to observe that the phase changes during the evolution, but the physical mechanics for this phenomenon are still obscure.

3.2 Evolution for the initially strong modulated wave train

The previous section discussed the evolution of wave trains with initial small disturbances. For these cases, because of the length limitation of the flume, the later stage of the modulation can not be observed. In this section, the evolution of a wave train with initial large disturbances ($a_{\pm}/a_0 = 0.5$) will be investigated.

The evolution of the surface elevations for the wave train ($\varepsilon = 0.11$, $f_c = 1.25$ Hz, and $\delta f = 0.10$ Hz) is shown in Fig. 10(a). Intermittent breaking was observed during the evolution, as shown in this figure, and the local extreme steepness ε of the breaking is approximately 0.427 ($\varepsilon = k_p a_m$, where k_p is the local wave number corresponding to the peak amplitude and a_m is the peak crest). Because the imposed sidebands are large, the evolution of this case is fast. The evolution of the surface elevation illustrates an approximate recurrence-type in the time domain. From Fig. 10(a), the number of waves in one modulation period at the locations near the wavemaker is 13 but decreases to 12 and then to 11 during the breaking region. However, outside the breaking region, the number of waves

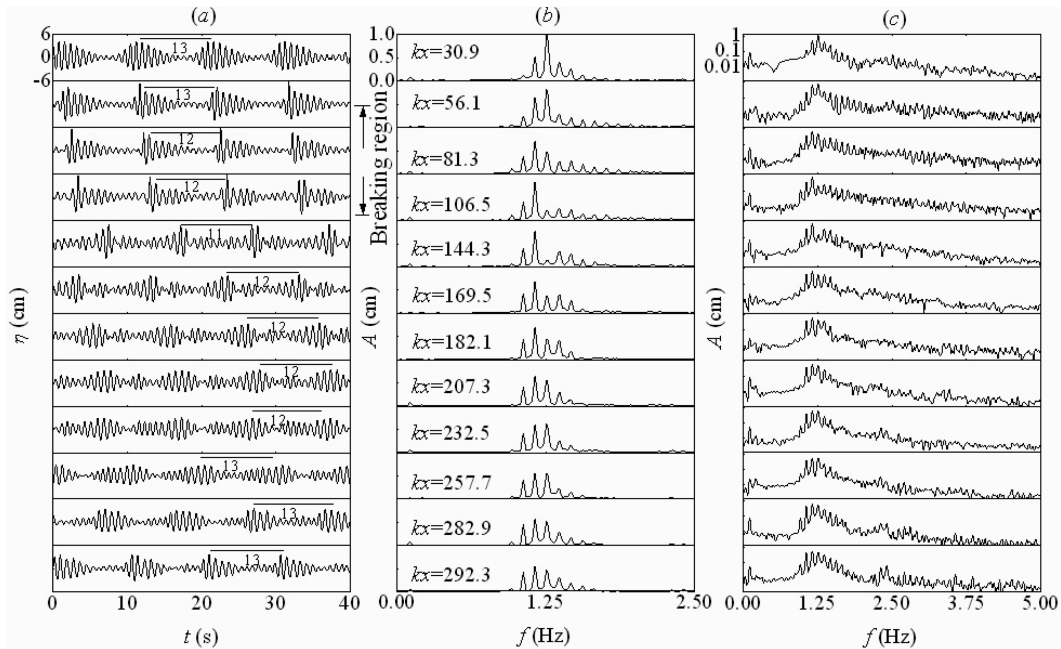


Fig. 10 The wave spectrum evolution for the wave trains ($f_c = 1.25$ Hz, $\varepsilon = 0.11$, $\delta f = 0.15$ Hz and $a_{\pm}/a_0 = 0.5$): (a) surface elevations, (b) wave amplitude spectrum in the liner coordinates and (c) wave amplitude spectrum in the semi-log coordinates

gradually returns to 13. At the same time, the envelope shape of the waves at the end of the flume become similar to the initial shape. This process is similar to the result of Tulin and Waseda (1999), who observed a recurrent evolution without breaking in both time and frequency domain. For this experimental case, the evolution in time demonstrates is approximately recurrence-type. The evolution in the frequency domain does not show this recurrent phenomenon due to the breaking. In the breaking region, the waves at the primary and the upper sideband lost most of their energy, and the lower sideband wave were dominant, (i.e., frequency downshift occurred). It is noted that, at $kx = 232.5$, the peak frequency of the wave train transferred to f_c , indicating that the breaking induced frequency downshift is not permanent. This result is consistent with the observation of Chiang and Huwng (2007). In the later stage, the waves at $f_c - 2\delta f$ and f_c grow while diminishing the wave at $f_c - \delta f$ due to the nonlinear resonance interactions. At the end of the flume, although the amplitude of the initial carrier wave f_c is close to that of the initial lower sideband wave, the amplitude of the initial upper sideband wave is still small compared to the wave at $f_c - 2\delta f$. Thus, there is not a recurrence in the frequency domain.

The instantaneous frequency evolution of this case is illustrated in Fig. 11. Because the imposed

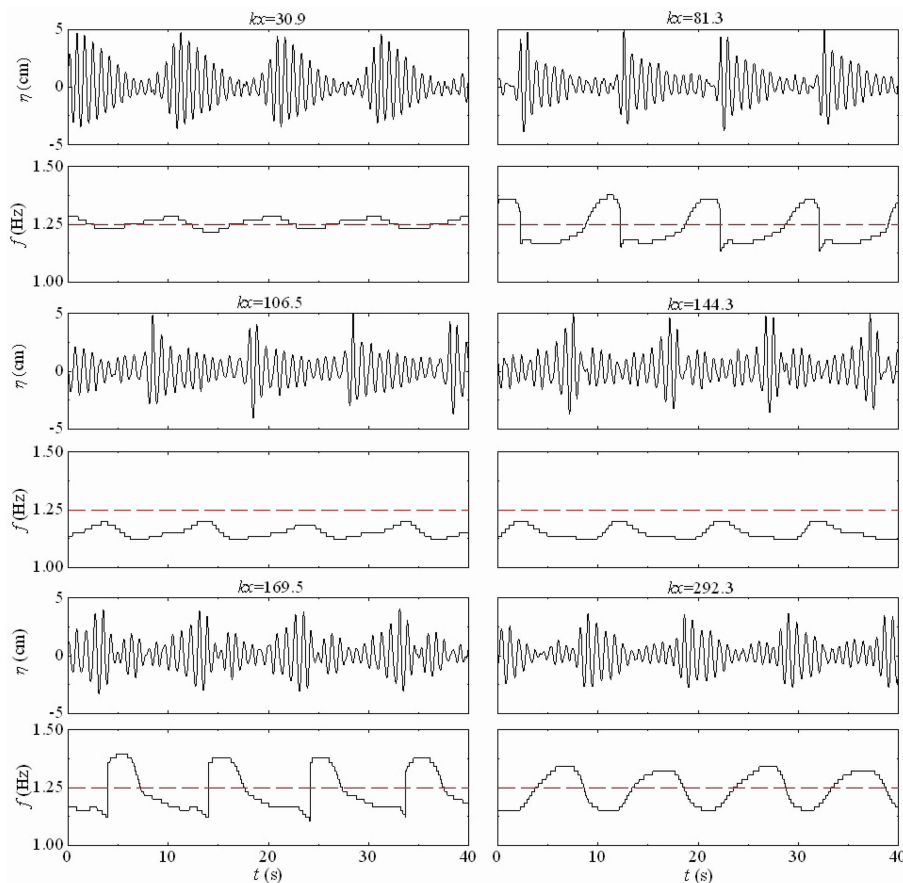


Fig. 11 The evolution of the instantaneous frequency for Case SB4 ($f_c = 1.25$ Hz, $\varepsilon = 0.13$, $\delta f = 0.1$ and $a_{\pm}/a_0 = 0.5$): The dashed line represents the initial peak wave frequency f_c

sidebands are large, the frequency modulation appears early. At the incipient breaking point ($kx = 81.3$), the frequency modulation is strong, with a gentle slope at the front of the modulation and a sharp decrease at the rear, and the dramatic decrease of the instantaneous frequencies correspond to surface elevations with very small amplitudes. After wave breaking, an effective frequency downshift occurred and the frequency modulation oscillates around the frequency of the lower sideband. However, the shape of the frequency modulation after the wave breaking is adverse of that in the upward locations, i.e., a steep front and a gentle rear. At the end of the flume, the frequency modulation returns to the shape at the locations near the wave maker. The frequency modulation oscillates around the input carrier frequency f_c again at the end of the flume ($kx = 292.3$), although the peak frequency at this location is $f_c - \delta f$.

4. Conclusions

New experiments regarding the modulational evolution of nonlinear wave trains were performed, which involved mechanically generating wave trains with different initial wave steepness, perturbed frequencies and initial modulation rates. The experimental results show that the development of the modulational instability relates closely to the initial wave steepness. With the growth of the initially imposed sidebands, free wave growth at $f_c \pm n\delta f$ ($n \geq 2$) was observed, especially for the waves with a frequency of $f_c + n\delta f$. For an increase of the initial steepness, the growth of the free waves has a tends to shift from select discrete frequencies to a continuous frequency band. During the wave evolution, breaking events were observed, and the local extreme wave steepness is approximately 0.43, which is similar to the values from previous studies on deep water wave breaking.

The Morlet wavelet transform was used herein to extract the instantaneous frequency of the wave trains. Due to the multi-scale analytical characteristics of the Morlet wavelet transform, the phase function of each wave components can also be obtained. The evolution of the instantaneous frequency illustrates that the frequency modulation increases with the growth of the sideband amplitude. At the middle and later stages of the modulation, the instantaneous frequencies are higher at the crests of the surface envelope and lower at the troughs of the envelope. Select abrupt frequency changes, which correspond to small wave amplitudes, were observed at the breaking regions. The wrapped phase functions demonstrate that, during the evolution, the phase of the upper sideband first deviates from the carrier wave at the beginning of the frequency modulation. However, at the later stage of the modulation, a deviation of the phases from the carrier wave is observed at the lower sideband.

The experiments with a pair of large imposed sidebands show an approximate recurrence in the time domain; however, mainly due to dissipation by breaking, the approximate recurrence evolution is not observed in the frequency domain. In the mean time, for this case, the frequency demonstrates an approximate recurrence type during the evolution.

Acknowledgments

This research is financially supported by the National Basic Research Program (Grant No. 2011CB013701), the National Nature Science Foundation (Grant Nos. 11172058, 51109032, 51009024), the China Postdoctoral Science Foundation (Grant No. 201104599) and the Open Foundation of State Key Laboratory of Hydrology-Water Resources and Hydraulic Engineering(2011490811).

References

- Banner, M.L. and Peirson, W.L. (2007), "Wave breaking onset and strength for two-dimensional deep-water wave groups", *J. Fluid Mech.*, **585**, 93-115.
- Banner, M.L. and Tian, X. (1998), "On the determination of the onset of breaking for modulating surface gravity waves", *J. Fluid Mech.*, **367**, 107-137.
- Benjamin, T.B. (1967), "Instability of periodic wavetrains in nonlinear dispersive systems", *Proceedings of the Royal Society of London Series A-Mathematical and Physical Sciences*.
- Benjamin, T.B. and Feir, J.E. (1967), "The disintegration of wave trains on deep water", *J. Fluid Mech.*, **27**(3), 417-430.
- Dysthe, K. (1979), "Note on a modification to the nonlinear Schrödinger equation for application to deep water waves", *Proceedings of the Royal Society of London Series A-Mathematical and Physical Sciences*.
- Farge, M. (1992), "Wavelet transforms and their applications to turbulence", *Annu. Rev. Fluid Mech.*, **24**, 395-457.
- Hammack, J.L. and Henderson, D.M. (1993), "Resonant interactions among surface-water waves", *Annu. Rev. Fluid Mech.*, **25**, 55-97.
- Hwung, H.H., Chiang, W.S. and Hsiao, S.C. (2007), "Observations on the evolution of wave modulation", *Proceedings of the Royal Society A-Mathematical Physical and Engineering Sciences*.
- Kharif, C., Kraenkel, R.A., Manna, M.A. and Thomas, R. (2010), "The modulational instability in deep water under the action of wind and dissipation", *J. Fluid Mech.*, **664**, 138-149.
- Lake, B.M., Yuen, H.C., Rungaldier, H. and Ferguson, W.E. (1977), "Nonlinear deep-water waves - theory and experiment .2. evolution of a continuous wave train", *J. Fluid Mech.*, **83**, 49-74.
- Lo, E. and Mei, C.C. (1985), "A numerical study of water-wave modulation based on a higher-order nonlinear schrödinger-equation", *J. Fluid Mech.*, **150**, 395-416.
- Longuet-Higgins, M.S. (1980), "Modulation of the amplitude of steep wind-waves", *J. Fluid Mech.*, **99**, 705-713.
- Ma, Y., Dong, G., Perlin, M., Ma, X., Wang, G. and Xu, J. (2010), "Laboratory observations of wave evolution, modulation and blocking due to spatially varying opposing currents", *J. Fluid Mech.*, **661**, 108-129.
- Massel, S.R. (2001), "Wavelet analysis for processing of ocean surface wave records", *Ocean Eng.*, **28**(8), 957-987.
- Melville, W.K. (1982), "The instability and breaking of deep-water waves", *J. Fluid Mech.*, **115**, 165-185.
- Melville, W.K. (1983), "Wave modulation and breakdown", *J. Fluid Mech.*, **128**, 489-506.
- Segur, H., Henderson, E., Carter, J., Hammack, J., Li, C.M., Pheiff, D. and Socha, K. (2005), "Stabilizing the benjamin-feir instability", *J. Fluid Mech.*, **539**, 229-271.
- Su, M.Y. (1982), "Three-dimensional deep-water waves. Part 1. Experimental measurements of skew and symmetric wave patterns", *J. Fluid Mech.*, **124**, 73-108.
- Tian, Z., Perlin, M. and Choi, W. (2008), "Evaluation of a deep-water breaking criterion", *Phys. Fluids.*, **20**, 066604.
- Tian, Z., Perlin, M. and Choi, W. (2010), "Energy dissipation in two-dimensional unsteady plunging breakers and an eddy viscosity model", *J. Fluid Mech.*, **655**, 217-257.
- Trulsen, K. and Dysthe, K.B. (1996), "A modified nonlinear schrodinger equation for broader bandwidth gravity waves on deep water", *Wave Motion*, **24**(3), 281-289.
- Tulin, M.P. and Waseda, T. (1999), "Laboratory observations of wave group evolution, including breaking effects", *J. Fluid Mech.*, **378**, 197-232.
- Waseda, T. and Tulin, M.P. (1999), "Experimental study of the stability of deep-water wave trains including wind effects", *J. Fluid Mech.*, **401**, 55-84.
- Zakharov, V.E. (1968), "Stability of periodic waves of finite amplitude on the surface of deep fluid", *J. Appl. Mech. Tech. Phys.*, **9**(2), 190-194.